ACS OMEGA

http://pubs.acs.org/journal/acsodf

Article

Purification and Sorting of Halloysite Nanotubes into Homogeneous, Agglomeration-Free Fractions by Polydopamine Functionalization

Cuneyt Erdinc Tas, Emine Billur Sevinis Ozbulut, Omer Faruk Ceven, Buket Alkan Tas, Serkan Unal, and Hayriye Unal*

Cite This: *ACS Omega* 2020, 5, 17962−17972

Read Online

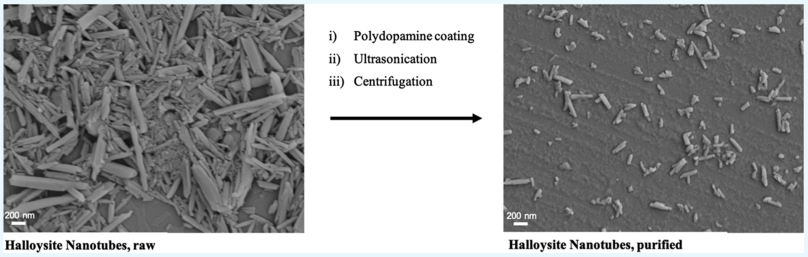

ABSTRACT: Halloysite nanotubes (HNTs) have attracted great attention in the field of nanotechnology as natural, high value-added nanomaterials. Despite their significant potential as carriers of active agents and fillers in nanocomposite structures, inhomogeneity of HNTs in terms of length and diameter along with their agglomeration tendency poses important obstacles for the utilization of them in a wider range of applications. Here, a facile, three-step separation protocol that allows the sorting of HNTs into agglomeration-free, uniform size fractions is reported. The protocol consists of coating of HNTs with polydopamine to impart hydrophilicity and aqueous dispersibility, followed by their ultrasonication and centrifugation at varying velocities for size-based separation. Particle size distribution analysis by scanning electron microscopy and dynamic light scattering has demonstrated that the separation protocol resulted in uniform HNT fractions of varying agglomeration states and particle sizes. The highest quality fraction obtained with 18% yield was free of agglomerations and consisted of HNTs of uniform lengths and diameters. The polydopamine coating on HNTs which facilitated the separation was demonstrated to be removed by a simple heat treatment that preserved the crystal structure of HNTs. The impact of the separation protocol on the loading and functionalization capacity of halloysites was investigated. Highest quality HNTs presented 4.1-fold increase in lumen loading and 1.9-fold increase in covalent surface coupling ratios compared to the loading and functionalization ratios obtained with raw HNTs. Similarly, sorted, high-quality HNTs were demonstrated to be better dispersed in a polymeric matrix, resulting in polymeric nanocomposites with significantly enhanced mechanical properties compared to nanocomposites prepared with raw HNTs. The three-step separation protocol presented here provides a toolbox that allows sorting of raw HNTs into uniform fractions of different size ranges, from which HNTs of desired qualities required by different applications can be selected.

INTRODUCTION

Halloysite nanotubes (HNTs) are abundant clay nanoparticles that have been utilized in a variety of scientific and industrial applications because of their intrinsic nanostructure, high thermal stability, acceptable mechanical strength, relatively low cost, and biocompatibility. HNTs present a natural hollow tubular structure composed of tetrahedral silicone dioxide outside and octahedral aluminum oxide inside along with a high aspect ratio and a low hydroxyl group density.[1] Their unique structural properties make HNTs notable as reinforcing fillers for polymers and also as containers for active components,[2,3] resulting in the utilization of HNTs in specific applications such as water purification,[4−6] drug delivery,[7,8] cancer cell isolation,[9,10] bone regeneration,[11,12] dentistry,[13,14] and cosmetics.[15,16]

HNTs naturally exist in a wide range of lengths and diameters.[17] Furthermore, they tend to agglomerate and cannot be individually dispersed in aqueous solutions and polymers. This inhomogeneity and agglomeration behavior of HNTs constitutes a significant limiting factor in the final properties of their nanocomposites, which prevents their full potential utilization. HNTs have been incorporated into

Received: March 9, 2020
Accepted: July 2, 2020
Published: July 17, 2020

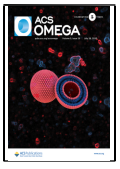

https://dx.doi.org/10.1021/acsomega.0c01057
ACS Omega 2020, 5, 17962−17972

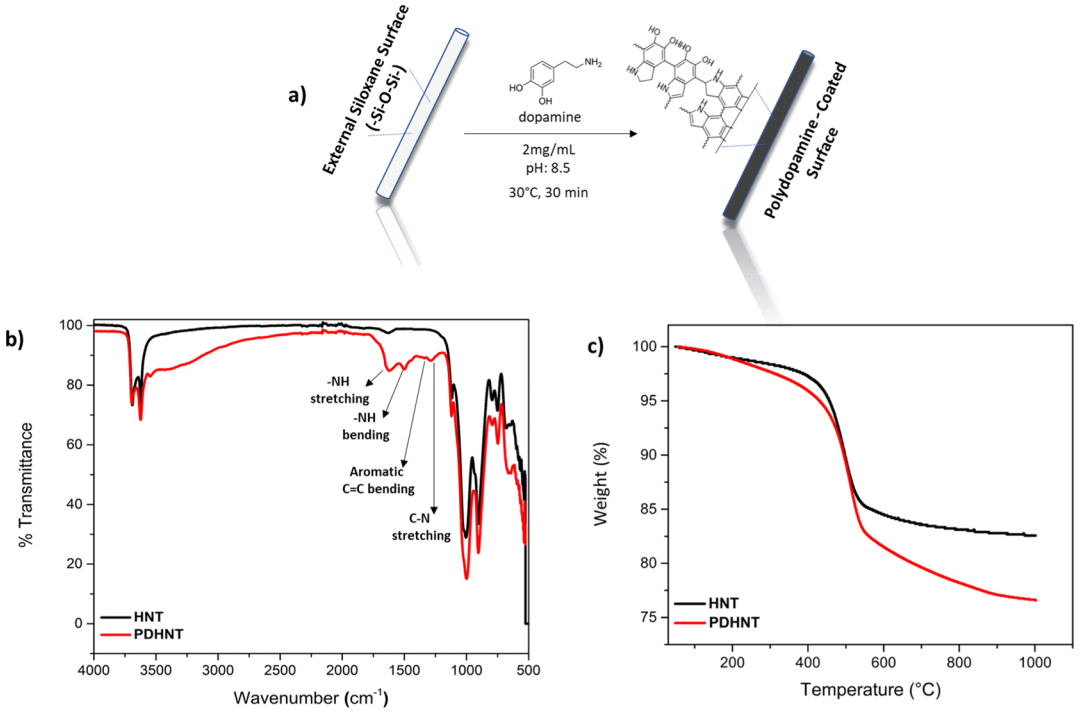

Figure 1. Coating of HNTs with polydopamine (a), FT-IR (b), and TGA (c) of raw HNTs and PDHNTs.

polymeric materials mainly to obtain polymer nanocomposites with enhanced mechanical and thermal properties. As for all polymeric nanocomposites, a homogeneous dispersion of the filler within the polymer matrix is one of the key requirements to achieve significant property improvements.[18−20] However, the agglomeration tendency of HNTs in the polymer matrix may lead to the deterioration of thermal and mechanical properties.[21−23] The utilization of agglomeration-free HNTs with a homogeneous size distribution in the nanoscale can improve their dispersion in the polymeric matrix and provide a homogeneous nanocomposite material. Furthermore, the wide distribution of the size of natural HNTs constitutes critical problems in certain applications. For example, very long HNTs above the average length can induce cell injury and inflammation when injected into cells for medical applications[24] or cause irritation to the skin in cosmetic applications.[25] Thus, a method that allows sorting of HNTs based on their size would improve their function and provide a toolbox for their efficient utilization in various applications.

A limited number of previous studies attempting the purification and size-separation of HNTs have focused on the ultrasonic scission of HNTs followed by a viscosity-based centrifugation where HNTs were dispersed in water in the presence of a polymeric material and a surfactant, providing high density and stability, respectively.[26,27] The potential of these methods might be limited because of the fact that these polymeric materials and surfactants cannot be completely removed at the end of the separation process and they might interfere with HNTs' functions.

Here, we demonstrate a facile method to obtain HNTs that are uniform in size and shape while preserving or improving their inherent properties. HNTs were functionalized with a polydopamine coating to impart hydrophilicity and enhance aqueous dispersibility, followed by ultrasonication and hydrophilicity gradient centrifugation that results in the purification of HNTs from other mineral impurities and sorting into different grades that are uniform in size and shape. The polydopamine coating that acts as an effective tool for the purification and separation of HNTs can be easily removed at the end of the separation process when needed. The proposed method provides a practical and useful way to obtain agglomeration free, uniform HNTs of desired aspect ratio which will allow the utilization of HNTs to their fullest potential.

RESULTS AND DISCUSSION

Polydopamine is a synthetic analogue to mussels' strong adhesive protein containing repeated amine and catechol groups that is obtained by the autoxidation of the dopamine monomer.[28] It is well-established that polydopamine coating is applicable to nearly all substrates to impart biocompatibility, post functionality, adhesion, and other targeted properties.[28−30] Polydopamine coating of HNT surfaces has been previously reported for their functionalization with nanoparticles and enzymes.[31−33]

The first step of the separation protocol was the coating of HNT surfaces with polydopamine in order to impart hydrophilicity and aqueous dispersibility for their centrifugation-based purification and separation. HNTs were simply mixed with the dopamine monomer in alkaline aqueous buffer which has mediated the self-polymerization of dopamine on the surface of HNTs (Figure 1a). The reaction mixture was then washed to remove unreacted dopamine and dried, resulting in polydopamine-coated HNTs (PDHNTs) in black powder form. The presence of the polydopamine coating on PDHNTs was demonstrated by Fourier transform infrared (FT-IR) spectroscopy (Figure 1b). Compared to raw HNTs' FT-IR spectrum, PDHNTs presented additional peaks appearing at 1337 cm^{-1} because of symmetric and asymmetric −NH stretching vibrations and peaks at 1625, 1499, and 1276 cm^{-1} corresponding to −NH bending, aromatic C═C bending, and C−N stretching, respectively,[34] confirming the

https://dx.doi.org/10.1021/acsomega.0c01057
ACS Omega 2020, 5, 17962−17972

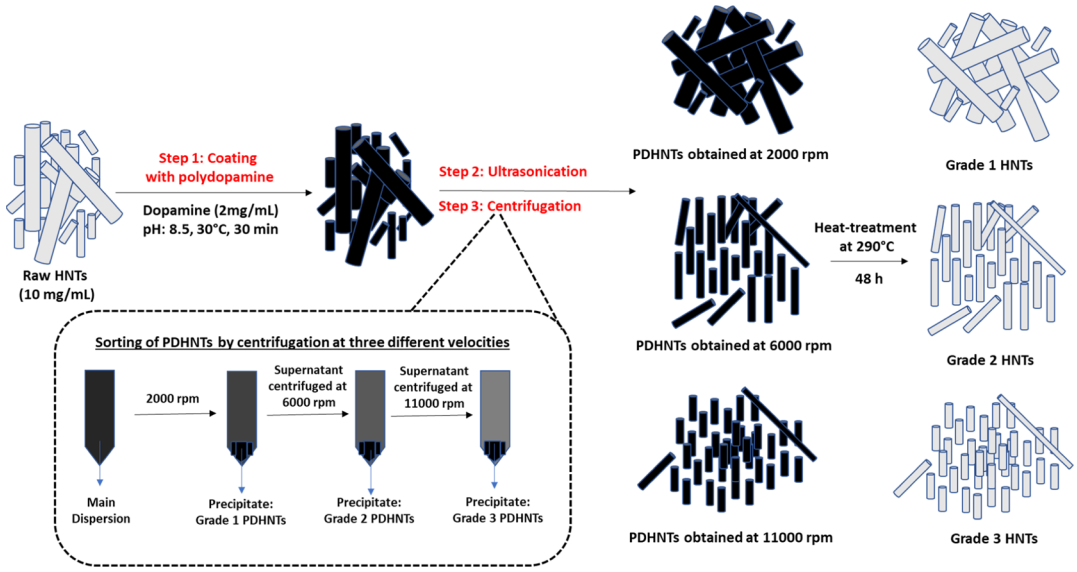

Figure 2. Schematic representation of the three-step separation protocol for HNTs.

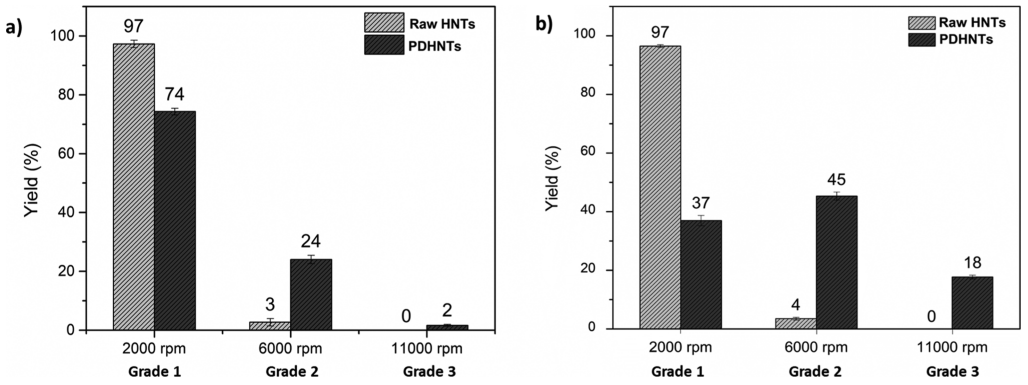

Figure 3. Yields of grade 1, grade 2, and grade 3 PDHNTs obtained at 2000, 6000, and 11,000 rpm centrifugation, respectively, in comparison to the yields of raw HNTs obtained by centrifugation at the same velocities. (a) Two-step separation protocol: polydopamine coating and centrifugation and (b) three-step separation: polydopamine coating, ultrasonication, and centrifugation.

presence of the polydopamine coating on HNTs. Figure 1c shows the thermogravimetric analysis (TGA) of raw HNTs and PDHNTs. Although both samples had similar decomposition behaviors, PDHNTs presented an additional weight loss of 5.9 wt % starting at 220 °C because of the decomposition of the polydopamine coating. These results further confirmed that HNT surfaces were successfully coated with polydopamine.

In the second step of the separation protocol, PDHNTs were treated with ultrasonication to break large agglomerations into individual nanotubes. Application of ultrasound energy is an effective and widely applied method to facilitate disruption of large particle agglomerates into nanosizes.[35] PDHNTs were treated with the optimal ultrasonication power and duration that minimize the destructive effect of ultrasound and also provide the sufficient energy to break up large agglomerations. In the third step of the separation, aqueous dispersions of ultrasonicated PDHNTs were subjected to consecutive centrifugations at increasing velocities. The precipitate obtained at 2000 rpm constituted grade 1 PDHNTs, where the supernatant was centrifuged again at 6000 rpm, resulting in the second precipitate constituting the grade 2 PDHNTs. The supernatant was further centrifuged at 11,000 rpm, and the third precipitate constituted grade 3 PDHNTs (Figure 2).

In order to assess the effect and importance of the polydopamine coating and ultrasonication steps on the separation efficiency of HNTs, the yields of grade 1, grade 2, and grade 3 PDHNTs obtained through (i) polydopamine coating alone and (ii) through both polydopamine coating and ultrasonication were calculated along with the yields of raw HNTs obtained through the same centrifugation conditions. Figure 3a demonstrates the yields of PDHNTs obtained through polydopamine coating of HNTs followed by centrifugation at varying velocities without the ultrasonication step in comparison to yields of raw HNTs that were processed through the same centrifugation protocol. Raw HNTs that were not functionalized with polydopamine did not show any separation as almost all raw HNTs (97.4 wt %) precipitated upon centrifugation at the lowest velocity of 2000 rpm, and negligible amount of HNTs remained in the supernatant. Large aggregates that are already present or have formed due to strong intermolecular interactions in raw HNTs have prevented the aqueous colloidal stability as expected. In contrast, when PDHNTs were dispersed in water without ultrasonication, they presented a significantly enhanced colloidal stability as only 74% of PDHNTs precipitated in the first centrifugation at 2000 rpm and 24% remained in the aqueous supernatant. Apparently, the polydopamine coating

https://dx.doi.org/10.1021/acsomega.0c01057
ACS Omega 2020, 5, 17962−17972

on HNTs has resulted in more stable aqueous dispersions of HNTs because of the highly hydrophilic character of the polydopamine.[36] While PDHNTs were able to be separated into different quality grades without the ultrasonication step, the efficiency of separation was very low. The improved hydrophilicity of PDHNTs improved the colloidal stability to a certain extent, but large agglomerations of PDHNTs that cannot be disintegrated limited the efficiency of the centrifugation-based separation.

On the other hand, when PDHNTs were further treated with the ultrasonication step, the yield of PDHNTs obtained at higher centrifugation velocities, which are supposedly the pure and agglomeration-free PDHNTs, has improved (Figure 3b). While the yield of grade 1 PDHNTs obtained at 2000 rpm centrifugation significantly decreased, the yield of grade 2 and grade 3 PDHNTs obtained at 6000 rpm and 11,000 rpm centrifugation increased and reached 45 and 18%, respectively. The increase in the yield of grade 2 and grade 3 qualities can be explained with the ultrasound scission stage that physically breaks down the PDHNT agglomerations through sound waves. The fact that 96.5% of raw HNTs without the polydopamine coating precipitated at 2000 rpm centrifugation and negligible yields were obtained at 6000 and 11,000 rpm demonstrates that the hydrophilicity imparted through the polydopamine coating is essential for the centrifugation-based separation of HNTs. As it can be clearly seen, when both polydopamine coating and ultrasound sonication were applied, the colloidal stability of PDHNTs was enhanced, which allowed the centrifugation-based separation of PDHNTs in increased yields.

The relationship between the amount of the polydopamine coating on HNTs and the aqueous colloidal stability it imparts to HNTs was investigated by comparing PDHNTs separated at different centrifugation velocities. Photographs of PDHNTs obtained by the three-step separation showed that different quality grades of PDHNT powders (Figure 4a) had different intensities of a black tint that is known to be caused by the polydopamine coating.[31] Although the initial PDHNT powder had a homogeneous black color, following the separation, grade 1, grade 2, and grade 3 PDHNTs had brown, gray, and black colors, respectively, demonstrating that different grades of HNTs possessed different amounts of polydopamine coating depending on their level of agglomeration. The amount of polydopamine coating on PDHNTs calculated by TGA further demonstrated that HNTs were inhomogeneously coated with polydopamine. Grade 1, grade 2, and grade 3 PDHNTs were calculated to have 1.51 wt %, 1.70 wt %, and 3.63 wt % polydopamine coating, respectively. Apparently, agglomeration-free, smaller HNTs were coated with polydopamine in higher percentages than HNTs in larger agglomerated forms, potentially because of larger surface areas of agglomeration-free HNTs relative to the surface areas of agglomerated HNTs. Thus, HNTs of different agglomeration states were imparted different extents of hydrophilic character and aqueous colloidal stability, which allowed the sorting of HNTs into different quality grades by a simple centrifugation.

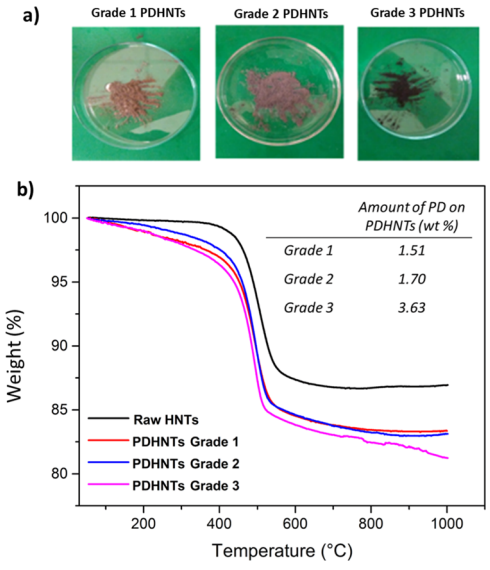

Figure 4. (a) Photographs of grade 1, grade 2, and grade 3 PDHNTs and (b) TGA of separated PDHNTs.

The size distribution and agglomeration state of PDHNTs obtained through the three-step separation protocol were characterized by scanning electron microscopy (SEM) and dynamic light scattering (DLS) analysis (Figure 5). Raw HNTs presented a wide distribution of nanotube lengths and diameters along with micron-sized aggregates of nanotubes. Following the three-step separation protocol, the polydisperse mixture of HNTs was separated into fractions of PDHNTs with more homogeneous distributions of sizes with minimum amount of aggregates. While grade 1 PDHNTs included longer nanotubes and occasional aggregates, grade 2 PDHNTs included shorter nanotubes and grade 3 PDHNTs included only individually separated nanotubes of shortest lengths (Figure 5a,b). Statistical analysis of PDHNT length distributions on the SEM images also demonstrated that the wide length distribution of raw HNTs ranging from 1200 to 400 nm was shifted to narrower distributions with significantly shorter average lengths for grade 2 and grade 3 PDHNTs (Figure 5c). The second step of the separation protocol which is the ultrasonication of PDHNTs to break large agglomerations resulted in the scission of nanotubes to different extents, as expected. Following the third step, which comprises the centrifugation of PDHNT dispersions at different velocities, PDHNTs were sorted based on their sizes where longest nanotubes were collected in grade 1 and shortest nanotubes were collected in grade 3. DLS analysis was also performed on aqueous dispersions for a qualitative comparison of length distributions and demonstrated a significant shift from wider length distributions at larger hydrodynamic diameters for raw HNTs to narrower distributions at shorter hydrodynamic diameters for grade 3 PDHNTs (Figure 5d). It is known that DLS cannot be safely used for the determination of actual lengths and diameters of nanotubular structures because it handles nanotubes as spherical particles within a hydrodynamic approximation. However, for well-dispersed individual nanotubes that can freely rotate, the length distributions obtained from DLS analysis are expected to corroborate well with actual length distributions. Thus, the agreement between DLS sizes and actual sizes can be interpreted, as the majority of the agglomerations present in the dispersion of pristine HNTs has been eliminated. While the DLS size distributions of raw HNTs did not match the size distributions obtained from SEM because of presence of large agglomerations, for separated grade 3 PDHNTs, both distributions were in good agreement, suggesting an agglomeration-free dispersion. These results further confirmed that the separation method provides a facile

https://dx.doi.org/10.1021/acsomega.0c01057
ACS Omega 2020, 5, 17962−17972

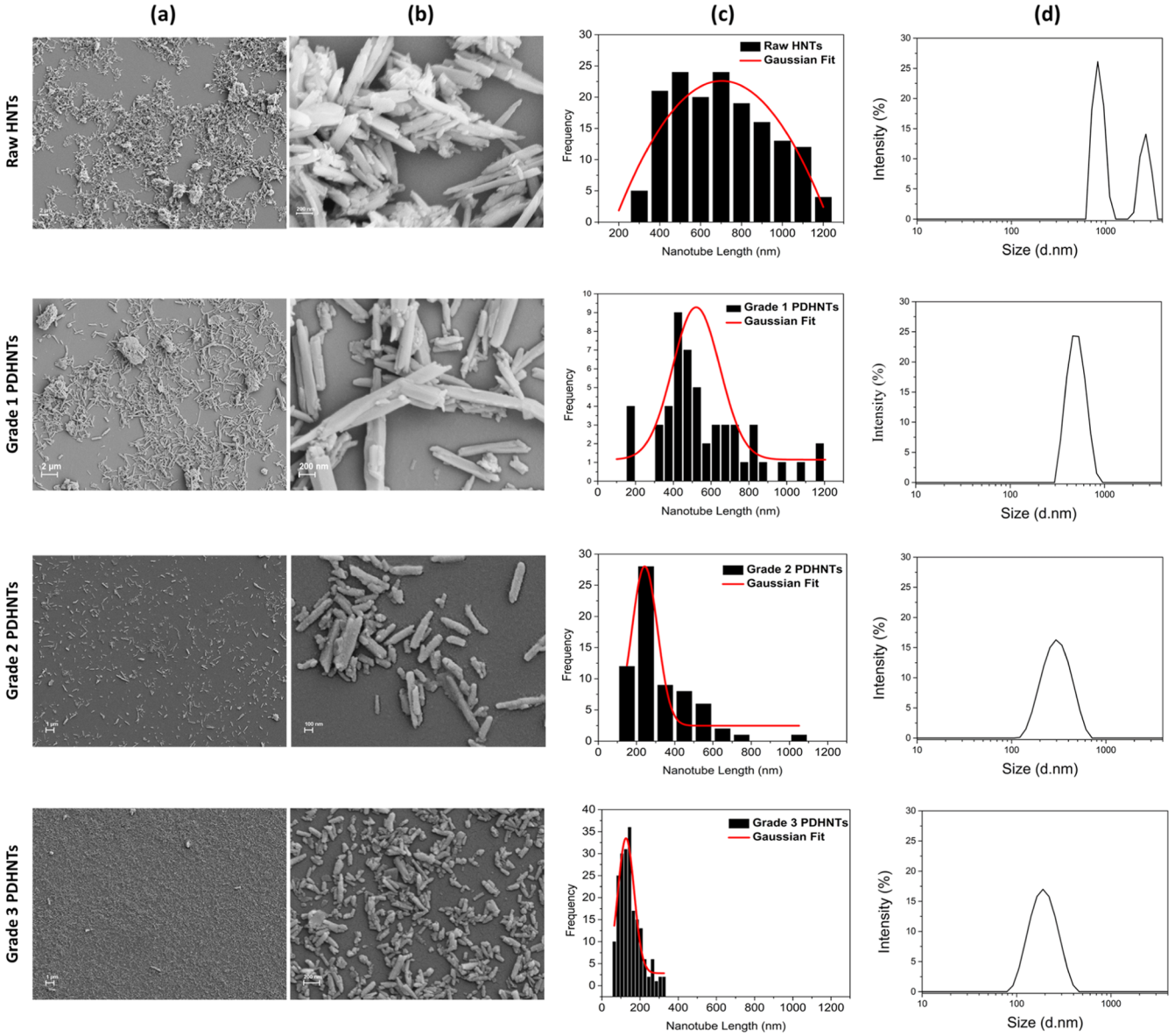

Figure 5. SEM and DLS characterization of raw HNTs and separated PDHNTs. (a) Representative SEM images at 10k magnification, (b) representative SEM images at 100k magnification, (c) nanotube length distribution histograms from SEM image analysis, and (d) size distribution histograms obtained by DLS.

route toward obtaining monodisperse and agglomeration-free fractions of HNTs from a polydisperse HNT mixture dominated by agglomerations.

The removability of the polydopamine coating on HNTs was investigated. In order to remove the polydopamine coating, separated PDHNTs were heat-treated at 290° for 48 h under the ambient atmosphere. The removal of the polydopamine coating was confirmed by the disappearance of the black tint on HNTs (Figure S1a). Furthermore, TGA of PDHNTs that were heat-treated showed that all of the polydopamine coating was removed as the treated nanotubes presented a similar thermogravimetric behavior as raw HNTs (Figure S1b).

Figure 6a–d demonstrates the SEM and DLS analysis of grade 1, grade 2, and grade 3 HNTs obtained following the removal of the polydopamine coating. The heat treatment did not exert any damage on the tubular shape of HNTs, which retained their monodisperse and agglomeration-free morphology. The removal of the polydopamine coating by heat treatment did not negatively affect the aqueous dispersibility of separated HNTs (Figure 6e). Grade 1, grade 2, and grade 3 HNTs obtained with the three-step separation protocol followed by the polydopamine coating removal were easily dispersed in water and presented colloidal stability for at least 6 h. These results demonstrated that the three-step separation protocol to obtain uniform and agglomeration free HNT fractions can safely be followed with a heat treatment step to remove the polydopamine coating in cases where the polydopamine coating would interfere with the desired application.

The effect of the treatments applied during the three-step separation protocol and removal of the polydopamine coating on the crystal structure of HNTs was also investigated (Figure 7). The X-ray diffraction (XRD) pattern of raw HNTs reflected the characteristic crystal structure of Halloysite-10 Å, which included the (001) peak at 2θ of 11.91°, (100) peak at

https://dx.doi.org/10.1021/acsomega.0c01057
ACS Omega 2020, 5, 17962−17972

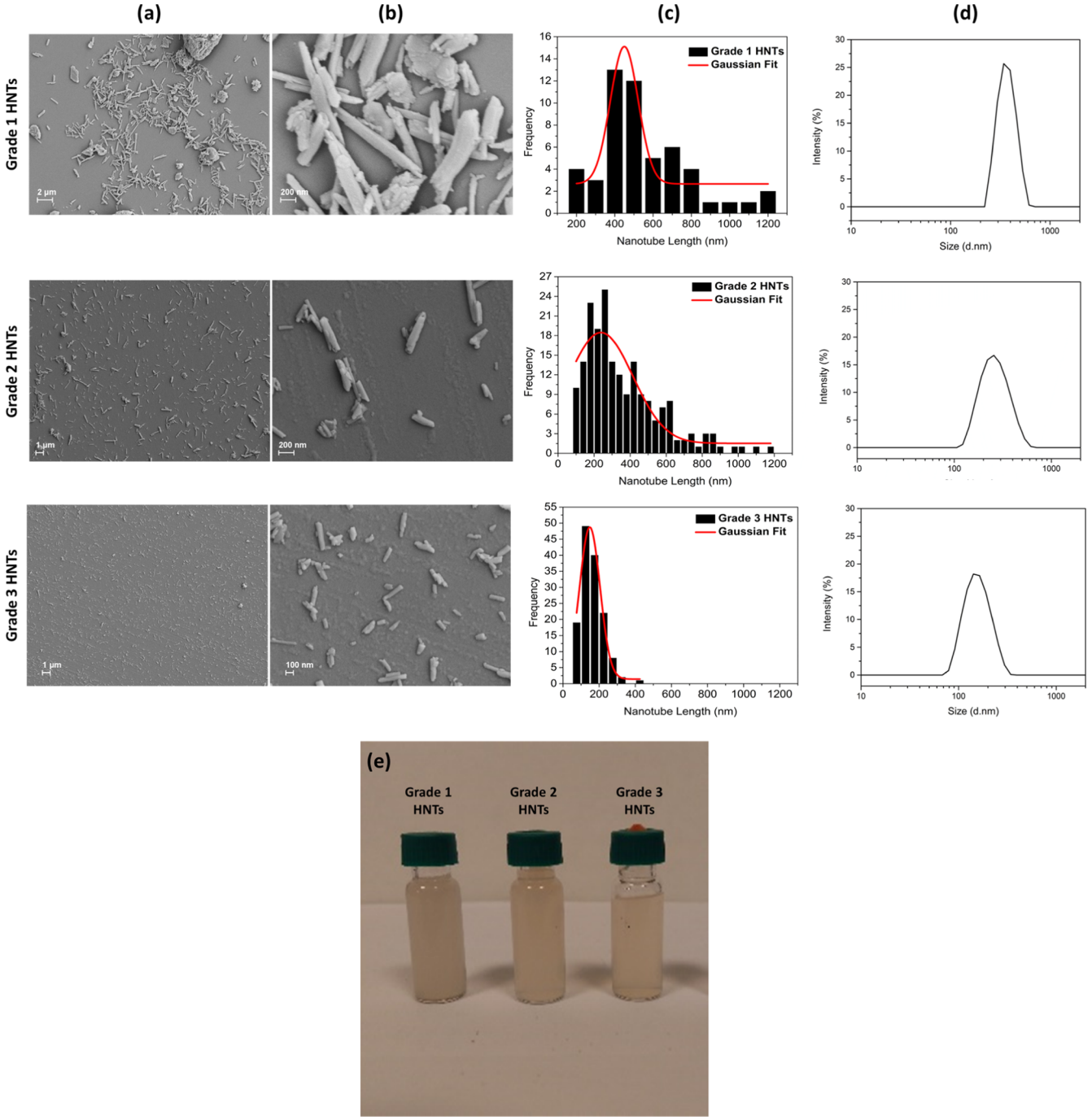

Figure 6. Analysis of grade 1, grade 2, and grade 3 HNTs following the removal of the polydopamine coating by heat treatment: (a) representative SEM images at 10k magnification, (b) representative SEM images at 100k magnification, (c) nanotube length distribution histograms from SEM image analysis, (d) size distribution histograms obtained by DLS, and (e) aqueous dispersions of HNTs after 6 h of storage at room temperature.

2θ of 20.17° indicative of the tubular halloysite structure, and the (002) peak at 2θ of 24.8°.[37] The XRD pattern of HNTs did not change following the treatments, indicating that the crystal structure of HNTs was not affected and their tubular nanostructure was retained. Furthermore, peaks corresponding to quartz (*) and kaolinite (#) impurities[17] visible in the patterns of raw HNTs and in grade 1 HNTs were not present in the XRD pattern of grade 2 and grade 3 HNTs, demonstrating that the three-step separation protocol also facilitated the purification of impurities in raw HNTs. The removal of impurities in HNTs via centrifugation of surfactant-assisted dispersions has been demonstrated before.[26,38] In our work, without the use of any surfactants, HNTs were well dispersed in water because of the polydopamine modification which allowed the centrifugation-based removal of nontubular clay impurities. These results demonstrated that the three-step separation protocol provides a tool for not only the preparation of agglomeration-free, monodisperse fractions but also the removal of impurities from raw HNTs.

The effect of the three-step separation on the covalent functionalization and loading capacity of HNTs was critical to understand. In order to investigate the loading capacity of separated HNTs obtained by the three-step separation method followed by the removal of the polydopamine coating, they

https://dx.doi.org/10.1021/acsomega.0c01057
ACS Omega 2020, 5, 17962−17972

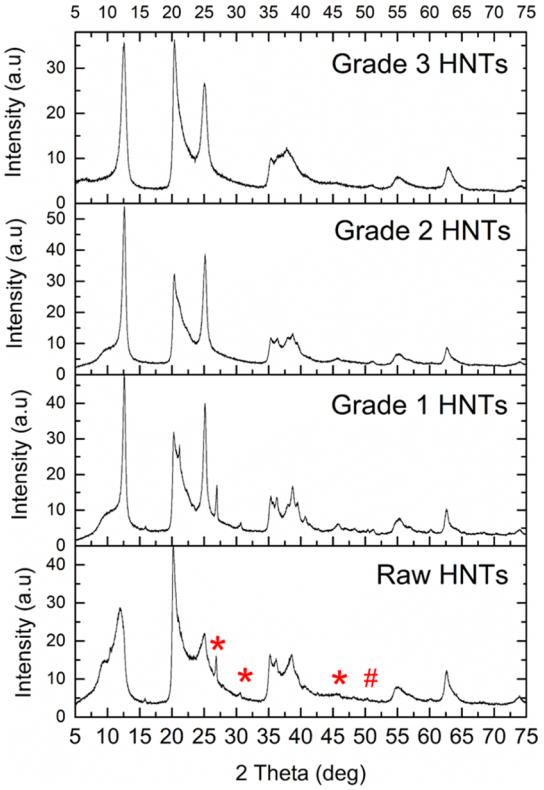

Figure 7. XRD analysis of raw HNTs; grade 1, grade 2, and grade 3 HNTs following the removal of the polydopamine coating.

were loaded with carvacrol as a representative active component through vacuum application. The weight percentage of the loaded carvacrol for separated HNTs was calculated through TGA (Figure 8a). Although raw HNTs were loaded with 5.8 wt % carvacrol, under the same experimental conditions, the loading capacity of grade 1 HNTs was slightly lower, where they were loaded with 3.5 wt % carvacrol. Apparently, grade 1 HNTs included an increased content of quartz and kaolinite impurities that had been observed in the XRD spectrum of both raw and grade 1 HNTs. On the other hand, the loading capacity of grade 2 and grade 3 HNTs significantly increased and reached 23.8 wt % for grade 3 HNTs which is 4 times higher than the loading capacity of unseparated raw HNTs. This significant increase in the loading capacity can be explained by the fact that grade 2 and 3 HNTs have been purified from agglomerated nanotubes and other impurities which cannot be loaded to their fullest capacity because of inadequate dispersion in carvacrol and reduced surface area. The three-step separation method provided an effective tool to obtain agglomeration-free and uniform HNTs that can be loaded with active materials at significantly higher contents that were not reported before.

The impact of the three-step separation on the covalent functionalization yield of HNTs was also investigated. The content of reactive hydroxyl groups on separated HNT surfaces was increased through alkaline treatment,[39] which were then reacted with sodium dodecyl sulfate (SDS) through a condensation reaction. The functionalization reaction was followed and verified by FT-IR analysis (Figure S2). The amount of covalently attached SDS on HNTs was determined by TGA (Figure 8b). Although raw HNTs were functionalized with SDS by 2.6 wt % only, grade 2 and grade 3 HNTs were functionalized by 4.4 wt % and 5.1 wt %, respectively. As the monodispersity of HNTs increased and agglomerations were minimized, more functional groups were available on the outer surface of HNTs, by which the functionalization efficiency increased more than two-fold compared to the functionalization rate of unprocessed raw HNTs. The relatively low yield for grade 3 HNTs may correspond to increased costs for such materials, despite the relatively low cost of commercially available raw HNTs. However, the three-step separation method presented in this study would now allow the use of these high-purity HNTs with significantly increased loading and functionalization capacities as well as better defined size distributions as nanocontainers in various high value-added applications such as active food packaging and drug delivery.

The effect of the monodisperse and agglomeration-free character of separated HNTs on the characteristics of polymeric HNT nanocomposites was also studied. HNTs separated into different quality grades and heat-treated for the removal of the polydopamine coating were incorporated into low-density polyethylene (LDPE) through melt compounding, and nanocomposite blown films were prepared. The HNT content in the prepared nanocomposite films was chosen to be 1 wt % as an optimum value based on our previous study that focused on the effect of the HNT content on LDPE-based nanocomposite film properties.[40] SEM visualization of resulting film surfaces demonstrated that the separation process applied to raw HNTs positively affected the dispersion quality of HNTs within the polymer matrix (Figure 9a). While nanocomposite films containing raw HNTs presented an inhomogeneous distribution of nanoparticles with several agglomerations, nanocomposite films prepared with grade 2 and grade 3 HNTs presented a significantly better dispersion

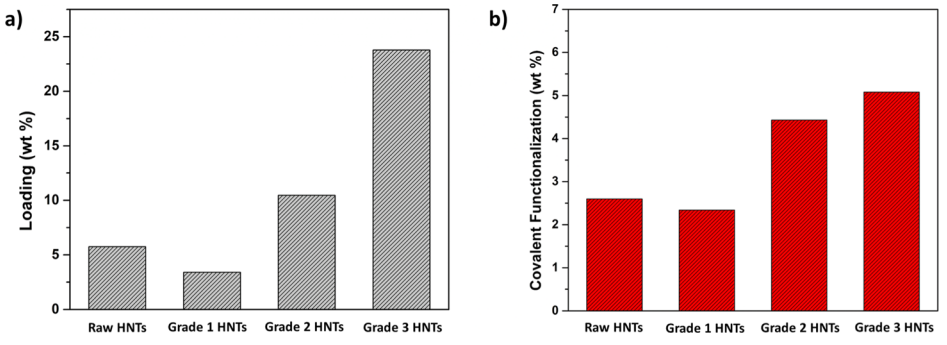

Figure 8. Functionalization yields of separated HNTs of different quality grades along with raw HNTs calculated by TGA. (a) Yields of loading with carvacrol. (b) Yields of covalent functionalization with SDS.

https://dx.doi.org/10.1021/acsomega.0c01057
ACS Omega 2020, 5, 17962−17972

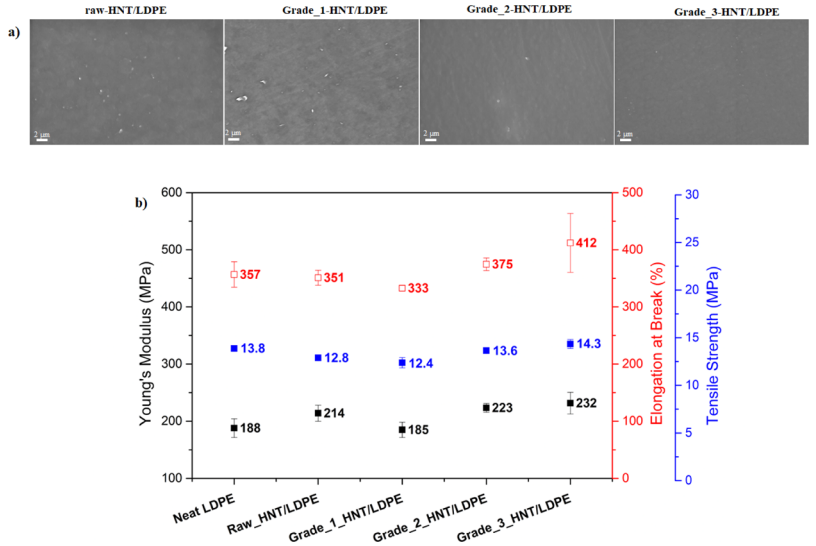

Figure 9. (a) SEM images of surfaces of nanocomposite films composed of LDPE and HNTs and (b) mechanical parameters of HNT/LDPE nanocomposite films containing different quality grade HNTs in comparison to neat LDPE films.

in the LDPE matrix. The films containing the highest quality HNT fraction, grade 3 HNTs, were almost free of agglomerations. The improved dispersibility of higher quality monodisperse HNTs has also positively impacted the mechanical properties of resulting nanocomposite films (Figure 9b). While nanocomposite films prepared with raw HNTs did not present any improvement in Young's modulus, tensile strength, and elongation at break values compared to neat LDPE films, the mechanical properties of nanocomposite films improved as a function of the separated HNT grade quality when compared to raw HNT reinforced nanocomposite films. Compared to less uniformly dispersed, agglomerated raw HNTs and grade 1 HNTs present in the LDPE matrix as evidenced by SEM analysis, the uniform dispersion of individual, significantly less agglomerated grade 2 and grade 3 HNTs resulted in the improvement of Young's modulus and the tensile strength, demonstrating the true nanoscale reinforcement effect.

CONCLUSIONS

HNTs were successfully separated into monodisperse, agglomeration-free fractions of different sizes through a facile three-step separation process that includes (i) coating of HNT surfaces with polydopamine, (ii) ultrasonication, and (iii) hydrophilicity-based centrifugation. The polydopamine coating on the surface of HNTs imparted hydrophilicity and aqueous dispersibility, which allowed the sorting of HNTs via centrifugation. Following the separation process, the polydopamine coating was completely removed through a simple heat treatment step. Resulting fractions of HNTs were demonstrated to be uniform in size and shape and preserved their intact nanotubular forms and crystal structures. The method allowed the sorting of raw polydisperse HNTs into fractions of different quality grades based on the velocity of centrifugation; while grade 1 HNTs obtained at low centrifugation velocity presented larger diameters with more agglomerations, grade 3 HNTs obtained at higher centrifugation velocity presented smaller diameters with almost no agglomerations. High-quality grade HNTs obtained through the separation protocol were shown to present significantly higher lumen loading and covalent surface functionalization capacity compared to raw HNTs. Furthermore, separated higher quality grade HNTs showed better dispersibility in a polymeric matrix, resulting in nanocomposite films with improved mechanical properties.

MATERIALS AND METHODS

Chemicals. Raw HNTs, SDS, sodium hydroxide pellets, and hydrochloric acid (ACS reagent, 37%) were purchased from Sigma-Aldrich Inc. Dopamine (3-hydroxytyramine hydrochloride) was purchased from Acros Organics Inc. Milli-Q purified water was used for all of the synthesis and characterization stages. Carvacrol was purchased from Tokyo Chemical Industry Co., LTD. Ultrapure Tris base (Tris-(hydroxymethyl)aminomethane) was purchased from MP Biomedicals, LLC. LDPE granules (PETİLEN F2-12) were provided by PETKİM Petrokimya A.Ş. All chemicals were used without any further purification.

Three-Step Separation of HNTs. HNTs were separated into three different grades of quality and size by following the three-step separation protocol. In the first step, HNTs were coated with polydopamine by dispersing 1 g of raw HNTs in 100 mL of purified water (10 mg/mL) with ultrasound sonication (Qsonica, Q700) for 30 min at 100% amplitude (120 W) with 5 s pulse on and 2 s pulse off in an ice bath. Following the sonication, 0.2 g of dopamine was added into the dispersion (2 mg/mL) and the pH was adjusted to 8.5 with Tris base powder. The prepared mixture was stirred at 30 °C for 30 min. Then, PDHNTs were separated from the reaction mixture with centrifugation at 5000 rpm for 5 min. Separated PDHNTs were washed with water and centrifuged five times to remove residual Tris base or unreacted dopamine molecule from the product. Obtained PDHNTs were dried at 50 °C for 24 h in a vacuum oven.

In the second step, an aqueous PDHNT dispersion (20 mg/mL) was prepared using an Ultra-TURRAX T18 basic dispersion system at approximately 11,000 rpm for 30 min and ultrasonicated for 45 min at 100% amplitude (120 W) with 5 s pulse on and 2 s pulse off in an ice bath.

In the third step, obtained aqueous PDHNT dispersion was separated into three grades by applying centrifugation for 10 min at 2000 rpm. Following the 2000 rpm centrifugation, the precipitate was dried and labeled as "Grade 1 PDHNTs". The

https://dx.doi.org/10.1021/acsomega.0c01057
ACS Omega 2020, 5, 17962−17972

supernatant was centrifuged for 10 min at 6000 rpm, and the precipitate was dried and labeled as "Grade 2 PDHNTs". The supernatant was centrifuged at 11,000 rpm, and the precipitate was dried and labeled as "Grade 3 PDHNTs".

For the removal of the polydopamine coating, grade 1, grade 2, and grade 3 PDHNTs were heat-treated for 48 h at 290 °C.

Functionalization of HNT Surfaces with SDS. Prior to the functionalization, HNTs were treated with NaOH to increase the amount of hydroxyl groups on the nanoparticle surface. HNTs (0.2 g, 0.01 g/mL) were stirred in 20 mL of NaOH solution overnight and then washed with distilled water several times to remove residual NaOH. SDS (0.02 g) was added into 10 mL of distilled water and 5 μL of HCl (37%) was added dropwise; the mixture was stirred for 15 min for the protonation of sodium sulfate groups on SDS. Finally, 0.2 g of HNTs was gradually added into the mixture, and the reaction was continued for 18 h at 40 °C.[41] The final product was obtained by centrifugation at 6000 rpm, which was then washed five times with distilled water and dried in a vacuum oven for 24 h at 80 °C.

Loading of HNTs with Carvacrol. In order to load HNTs with carvacrol, 40 mg of HNTs was dispersed in 20 mL of carvacrol by using ultrasound sonication for 10 min at 60% amplitude (65 W) with 2 s pulse on and 5 s pulse off in an ice bath. Then, HNT−carvacrol dispersion was connected to a vacuum pump, and vacuum (2 mbar) was applied for 20 min. The vacuum was released to bring the system to the atmospheric pressure and then vacuum was reapplied under the same conditions. At the end of the two-step vacuum cycle, HNTs were separated from the excess amount of carvacrol by centrifugation at 5000 rpm for 5 min. Obtained carvacrol-loaded HNTs (CHNT) were washed with ethanol to remove the residual carvacrol from the HNT surface. Finally, CHNTs were dried at room temperature for 24 h.[42]

Preparation of Polyethylene−HNT Nanocomposite Films. A mixture of polyethylene (99 wt %) and HNT (1 wt %) powders was fed into a twin-screw extruder (Zamac Mercator with a screw diameter of 12 mm and L/D of 40) and processed at the zone temperature range between 160 and 180 °C with the screw speed of 300 rpm. Nanocomposite melt flowing from the extrusion die was cooled in a water bath and pelletized. Afterward, the pellet form of the nanocomposite mixture was transferred to a single screw film blowing machine (Scientific Laboratory Ultra Micro Film Blowing Line Type LUMF-150 with L8-30/C, LabTech Engineering), processed at 150−160 °C with a single screw speed of 80 rpm and blown into 55−65 μm thick films. The neat LDPE samples were processed through the blown film extrusion of LDPE granules under the same conditions.

Characterization Methods. TGA of all samples was performed using a Shimadzu Corp. DTG-60H (TGA/DTA) instrument by heating samples up to 1000 °C with a rate of 10 °C/min under nitrogen. Prior to the analysis, samples were dried for 30 min at 100 °C in the instrument to remove all moisture from the samples.

Determination of the hydrodynamic diameter of samples was performed using a DLS instrument (Zetasizer Nano—ZS, Malvern Instruments Ltd., UK) at 25 °C at a sample concentration of 2 mg/mL for each sample.

A Nicolet IS10 FT-IR spectroscope with an attenuated total reflection system was utilized for the chemical analysis of raw samples.

Phase purity of samples was analyzed by XRD using a Bruker D2 Phaser XRD instrument using Cu Kα radiation (K = 1.5418 Å, 40 kV, 200 mA) in the 2θ range of 5−70°.

The samples were visualized using a Zeiss LEO Supra 35VP scanning electron microscope. HNT samples were prepared for visualization on silicon wafer by drying a drop of aqueous HNT dispersions (0.1 mg/mL) obtained by ultrasonication for 2 min at 70% amplitude (75 W) with 5 s pulse on and 2 s pulse off in an ice bath. For the visualization of HNT/PE nanocomposite films, samples were coated with Au−Pd and images were recorded using a secondary electron detector at 5 kV under high vacuum. Size distribution of HNT specimens was analyzed using SEM images at 50k magnification by ImageJ software. For the statistical analysis, lengths were measured using at least 50−200 nanotubes for each grade, and they were presented as frequencies of nanotubes versus their lengths. The mechanical properties of nanocomposite films were investigated using a universal testing machine Zwick Roell Z100 UTM, with a load cell of 200 N and a crosshead speed of 12.5 mm min^{-1} according to the ASTM D1708-10 testing method. Dog-bone test specimens had a length of 38 mm and a width of 15 mm, a narrow section width of 5 mm, and a grip distance of 22 mm. An average of four replicates of each sample was reported. Thicknesses of films were measured using a digimatic micrometer (Mitutoyo Quicmike, no. 99MAB041M).

■ ASSOCIATED CONTENT

Supporting Information

The Supporting Information is available free of charge at https://pubs.acs.org/doi/10.1021/acsomega.0c01057.

Photographs and TGA of separated HNTs following the removal of the polydopamine coating and FT-IR spectra of SDS-functionalized HNTs (PDF)

■ AUTHOR INFORMATION

Corresponding Author

Hayriye Unal − *Sabanci University SUNUM Nanotechnology Research Center, 34956 Istanbul, Turkey;* orcid.org/0000-0002-9090-2440; Email: hunal@sabanciuniv.edu

Authors

Cuneyt Erdinc Tas − *Faculty of Engineering and Natural Sciences, Sabanci University, 34956 Istanbul, Turkey; Sabanci University SUNUM Nanotechnology Research Center, 34956 Istanbul, Turkey;* orcid.org/0000-0001-8390-1434

Emine Billur Sevinis Ozbulut − *Faculty of Engineering and Natural Sciences, Sabanci University, 34956 Istanbul, Turkey*

Omer Faruk Ceven − *Faculty of Technology, Marmara University, 34722 Istanbul, Turkey*

Buket Alkan Tas − *Faculty of Engineering and Natural Sciences, Sabanci University, 34956 Istanbul, Turkey; Sabanci University SUNUM Nanotechnology Research Center, 34956 Istanbul, Turkey*

Serkan Unal − *Faculty of Engineering and Natural Sciences and Integrated Manufacturing Technologies Research and Application Center, Sabanci University, 34956 Istanbul, Turkey;* orcid.org/0000-0003-4423-6202

Complete contact information is available at: https://pubs.acs.org/10.1021/acsomega.0c01057

https://dx.doi.org/10.1021/acsomega.0c01057
ACS Omega 2020, 5, 17962−17972

Notes

The authors declare no competing financial interest.

■ ACKNOWLEDGMENTS

This work was supported by the Scientific and Technological Research Council of Turkey (TUBITAK) under the project number 216M012.

■ REFERENCES

(1) Zhang, Y.; Tang, A.; Yang, H.; Ouyang, J. Applications and interfaces of halloysite nanocomposites. *Appl. Clay Sci.* **2016**, *119*, 8−17.
(2) Shchukina, E.; Shchukin, D. G. Nanocontainer-Based Active Systems: From Self-Healing Coatings to Thermal Energy Storage. *Langmuir* **2019**, *35*, 8603−8611.
(3) Cavallaro, G.; Lazzara, G.; Milioto, S.; Parisi, F.; Evtugyn, V.; Rozhina, E.; Fakhrullin, R. Nanohydrogel formation within the halloysite lumen for triggered and sustained release. *ACS Appl. Mater. Interfaces* **2018**, *10*, 8265−8273.
(4) Peng, Q.; Liu, M.; Zheng, J.; Zhou, C. Adsorption of dyes in aqueous solutions by chitosan−halloysite nanotubes composite hydrogel beads. *Microporous Mesoporous Mater.* **2015**, *201*, 190−201.
(5) Ormanci-Acar, T.; Celebi, F.; Keskin, B.; Mutlu-Salmanlı, O.; Agtas, M.; Turken, T.; Tufani, A.; Imer, D. Y.; Ince, G. O.; Demir, T. U.; Menceloglu, Y. Z.; Unal, S.; Koyuncu, I. Fabrication and characterization of temperature and pH resistant thin film nanocomposite membranes embedded with halloysite nanotubes for dye rejection. *Desalination* **2018**, *429*, 20−32.
(6) Papoulis, D.; Panagiotaras, D.; Tsigrou, P.; Christoforidis, K. C.; Petit, C.; Apostolopoulou, A.; Stathatos, E.; Komarneni, S.; Koukouvelas, I. Halloysite and sepiolite−TiO2 nanocomposites: Synthesis characterization and photocatalytic activity in three aquatic wastes. *Mater. Sci. Semicond. Process.* **2018**, *85*, 1−8.
(7) Lun, H.; Ouyang, J.; Yang, H. Natural halloysite nanotubes modified as an aspirin carrier. *RSC Adv.* **2014**, *4*, 44197−44202.
(8) Liu, H.; Wang, Z.-G.; Liu, S.-L.; Yao, X.; Chen, Y.; Shen, S.; Wu, Y.; Tian, W. Intracellular pathway of halloysite nanotubes: potential application for antitumor drug delivery. *J. Mater. Sci.* **2019**, *54*, 693−704.
(9) Hughes, A. D.; King, M. R. Use of naturally occurring halloysite nanotubes for enhanced capture of flowing cells. *Langmuir* **2010**, *26*, 12155−12164.
(10) Li, X.; Chen, J.; Liu, H.; Deng, Z.; Li, J.; Ren, T.; Huang, L.; Chen, W.; Yang, Y.; Zhong, S. *β*-Cyclodextrin coated and folic acid conjugated magnetic halloysite nanotubes for targeting and isolating of cancer cells. *Colloids Surf., B* **2019**, *181*, 379−388.
(11) Lvov, Y. M.; DeVilliers, M. M.; Fakhrullin, R. F. The application of halloysite tubule nanoclay in drug delivery. *Expert Opin. Drug Delivery* **2016**, *13*, 977−986.
(12) Huang, K.; Ou, Q.; Xie, Y.; Chen, X.; Fang, Y.; Huang, C.; Wang, Y.; Gu, Z.; Wu, J. Halloysite Nanotube Based Scaffold for Enhanced Bone Regeneration. *ACS Biomater. Sci. Eng.* **2019**, *5*, 4037−4047.
(13) Alkatheeri, M. S.; Palasuk, J.; Eckert, G. J.; Platt, J. A.; Bottino, M. C. Halloysite nanotube incorporation into adhesive systems—effect on bond strength to human dentin. *Clin. Oral Invest.* **2015**, *19*, 1905−1912.
(14) Monteiro, J. C.; Garcia, I. M.; Leitune, V. C. B.; Visioli, F.; de Souza Balbinot, G.; Samuel, S. M. W.; Makeeva, I.; Collares, F. M.; Sauro, S. Halloysite nanotubes loaded with alkyl trimethyl ammonium bromide as antibacterial agent for root canal sealers. *Dent. Mater.* **2019**, *35*, 789−796.
(15) Suh, Y. J.; Kil, D. S.; Chung, K. S.; Abdullayev, E.; Lvov, Y. M.; Mongayt, D. Natural Nanocontainer for the Controlled Delivery of Glycerol as a Moisturizing Agent. *J. Nanosci. Nanotechnol.* **2011**, *11*, 661−665.
(16) Cavallaro, G.; Milioto, S.; Konnova, S.; Fakhrullina, G.; Akhatova, F.; Lazzara, G.; Fakhrullin, R.; Lvov, Y. Halloysite/keratin nanocomposite for human hair photoprotection coating. *ACS Appl. Mater. Interfaces* **2020**, *12*, 24348−24362.
(17) Joussein, E.; Petit, S.; Churchman, J.; Theng, B.; Righi, D.; Delvaux, B. Halloysite clay minerals − a review. *Clay Miner.* **2005**, *40*, 383−426.
(18) Du, M.; Guo, B.; Jia, D. Newly emerging applications of halloysite nanotubes: a review. *Polym. Int.* **2010**, *59*, 574−582.
(19) Kausar, A. Review on Polymer/Halloysite Nanotube Nanocomposite. *Polym.-Plast. Technol. Eng.* **2018**, *57*, 548−564.
(20) Liu, M.; Jia, Z.; Jia, D.; Zhou, C. Recent advance in research on halloysite nanotubes-polymer nanocomposite. *Prog. Polym. Sci.* **2014**, *39*, 1498−1525.
(21) Makaremi, M.; De Silva, R. T.; Pasbakhsh, P. Electrospun Nanofibrous Membranes of Polyacrylonitrile/Halloysite with Superior Water Filtration Ability. *J. Phys. Chem. C* **2015**, *119*, 7949−7958.
(22) Gaaz, T. S.; Sulong, A. B.; Kadhum, A. A. H.; Nassir, M. H.; Al-Amiery, A. A. Absolute variation of the mechanical characteristics of halloysite reinforced polyurethane nanocomposites complemented by Taguchi and ANOVA approaches. *Results Phys.* **2017**, *7*, 3287−3300.
(23) Liu, W.; Hoa, S.; Pugh, M. Fracture toughness and water uptake of high-performance epoxy/nanoclay nanocomposites. *Compos. Sci. Technol.* **2005**, *65*, 2364−2373.
(24) Lvov, Y.; Abdullayev, E. Functional polymer−clay nanotube composites with sustained release of chemical agents. *Prog. Polym. Sci.* **2013**, *38*, 1690−1719.
(25) López-Galindo, A.; Viseras, C.; Cerezo, P. Compositional, technical and safety specifications of clays to be used as pharmaceutical and cosmetic products. *Appl. Clay Sci.* **2007**, *36*, 51−63.
(26) Rong, R.; Xu, X.; Zhu, S.; Li, B.; Wang, X.; Tang, K. Facile preparation of homogeneous and length controllable halloysite nanotubes by ultrasonic scission and uniform viscosity centrifugation. *Chem. Eng. J.* **2016**, *291*, 20−29.
(27) Zhao, J. M.; Chang, J. H.; Lee, Y. K.; Hwang, K. H.; Lee, J. K. Separation of Halloysite Nano Tubes (HNTs) by Homogenization of Quartz Contaminated Kaolins. *J. Nanosci. Nanotechnol.* **2019**, *19*, 984−987.
(28) Liu, Y.; Ai, K.; Lu, L. Polydopamine and Its Derivative Materials: Synthesis and Promising Applications in Energy, Environmental, and Biomedical Fields. *Chem. Rev.* **2014**, *114*, 5057−5115.
(29) Zhan, Y.; Zhang, J.; Wan, X.; Long, Z.; He, S.; He, Y. Epoxy composites coating with Fe3O4 decorated graphene oxide: Modified bio-inspired surface chemistry, synergistic effect and improved anticorrosion performance. *Appl. Surf. Sci.* **2018**, *436*, 756−767.
(30) Zhan, Y.; He, S.; Wan, X.; Zhao, S.; Bai, Y. Thermally and chemically stable poly(arylene ether nitrile)/halloysite nanotubes intercalated graphene oxide nanofibrous composite membranes for highly efficient oil/water emulsion separation in harsh environment. *J. Membr. Sci.* **2018**, *567*, 76−88.
(31) Chao, C.; Liu, J.; Wang, J.; Zhang, Y.; Zhang, B.; Zhang, Y.; Xiang, X.; Chen, R. Surface Modification of Halloysite Nanotubes with Dopamine for Enzyme Immobilization. *ACS Appl. Mater. Interfaces* **2013**, *5*, 10559−10564.
(32) Liu, Y.; Guan, H.; Zhang, J.; Zhao, Y.; Yang, J.-H.; Zhang, B. Polydopamine-coated halloysite nanotubes supported AgPd nanoalloy: An efficient catalyst for hydrolysis of ammonia borane. *Int. J. Hydrogen Energy* **2018**, *43*, 2754−2762.
(33) Feng, J.; Fan, H.; Zha, D.-a.; Wang, L.; Jin, Z. Characterizations of the Formation of Polydopamine-Coated Halloysite Nanotubes in Various pH Environments. *Langmuir* **2016**, *32*, 10377−10386.
(34) Zhu, B.; Edmondson, S. Polydopamine-melanin initiators for Surface-initiated ATRP. *Polymer* **2011**, *52*, 2141−2149.
(35) Taurozzi, J. S.; Hackley, V. A.; Wiesner, M. R. Ultrasonic dispersion of nanoparticles for environmental, health and safety assessment−issues and recommendations. *Nanotoxicology* **2011**, *5*, 711−729.
(36) Lynge, M. E.; van der Westen, R.; Postma, A.; Städler, B. Polydopamine—a nature-inspired polymer coating for biomedical science. *Nanoscale* **2011**, *3*, 4916−4928.

https://dx.doi.org/10.1021/acsomega.0c01057
ACS Omega 2020, 5, 17962−17972

(37) Gaaz, T.; Sulong, A.; Kadhum, A.; Nassir, M.; Al-Amiery, A. Impact of Sulfuric Acid Treatment of Halloysite on Physico-Chemic Property Modification. *Materials* **2016**, *9*, 620.
(38) Liu, M.; Cao, X.; Liu, H.; Yang, X.; Zhou, C. 12—Halloysite-Based Polymer Nanocomposites. In *Nanomaterials from Clay Minerals*; Wang, A., Wang, W., Eds.; Elsevier, 2019; pp 589−626.
(39) Zeng, S.; Reyes, C.; Liu, J.; Rodgers, P. A.; Wentworth, S. H.; Sun, L. Facile hydroxylation of halloysite nanotubes for epoxy nanocomposite applications. *Polymer* **2014**, *55*, 6519−6528.
(40) Tas, C. E.; Hendessi, S.; Baysal, M.; Unal, S.; Cebeci, F. C.; Menceloglu, Y. Z.; Unal, H. Halloysite Nanotubes/Polyethylene Nanocomposites for Active Food Packaging Materials with Ethylene Scavenging and Gas Barrier Properties. *Food Bioprocess Technol.* **2017**, *10*, 789−798.
(41) Suppiah, K.; Teh, P. L.; Husseinsyah, S.; Rahman, R. Properties and characterization of carboxymethyl cellulose/halloysite nanotube bio-nanocomposite films: Effect of sodium dodecyl sulfate. *Polym. Bull.* **2019**, *76*, 365−386.
(42) Alkan Tas, B.; Sehit, E.; Erdinc Tas, C.; Unal, S.; Cebeci, F. C.; Menceloglu, Y. Z.; Unal, H. Carvacrol loaded halloysite coatings for antimicrobial food packaging applications. *Food Packag. Shelf Life* **2019**, *20*, 100300.

https://dx.doi.org/10.1021/acsomega.0c01057
ACS Omega 2020, 5, 17962−17972